ELSEVIER

Chemical Physics 207 (1996) 245–259

Chemical Physics

F–D_2 state resolved reactive scattering at 180 and 240 meV collision energies. II. Quasi-classical cross sections. A comparison with the experimental results

F.J. Aoiz [a], L. Bañares [a], M. Faubel [b], B. Martínez-Haya [b], L.Y. Rusin [b], U. Tappe [b], J.P. Toennies [b]

[a] *Departamento de Química Física, Facultad de Química, Universidad Complutense, 28040 Madrid, Spain*
[b] *Max-Planck-Institut für Strömungsforschung, Bunsenstrasse 10, D-37073 Göttingen, Germany*

Received 7 September 1995

Abstract

Quasi-classical trajectory calculations (QCT) have been carried out for the F+D_2 reaction at the collision energies and initial rotational states necessary to simulate the molecular beam results presented in the preceding paper of this issue by Faubel et al. Although the general trends are well accounted for by the QCT calculations, there are significant differences between experiment and theoretical results. The vibrational resolved differential cross section are in an overall good agreement; however, the QCT calculations clearly underestimate both backward and forward scattering. The comparison between the product state distributions indicates that the QCT ones are somewhat broader than the experimental ones for most of the vibrational states. The limitations of the theoretical results become more clear when the laboratory frame (LAB) angular distributions (AD) and time-of-flight (TOF) spectra are simulated using the calculated DCS resolved into the final rovibrational states, v_f, j_f. The theoretical findings and, especially, the roles of translational energy and initial rotational momentum on the dynamics of this reaction are discussed in some detail.

1. Introduction

The F+H_2 is one of the most extensively studied chemical reactions from the dymamical point of view. About a decade ago, a milestone in the study of the prototypic F+H_2 reactive system was established by the famous high resolution molecular beam experiments of Lee and coworkers [1,2], yielding vibrationally state-resolved differential cross sections (DCS) for the F+H_2, F+D_2, and F+HD isotopic variants of the reaction. These measurements show the appearance of forward peaks (the forward direction defined by the incoming F atom in the center-of-mass (CM) system) in DCS for the scattering of HF(v_f = 3) from the F+H_2 reactive encounters in the collision energy (E_{cm}) range between 80 and 150 meV (1 meV = 0.096473 kJ mol^{-1}). A smaller forward peak was also observed in the scattering of DF(v_f = 4) from F+D_2 at E_{cm} = 144 meV. For the rest of the vibrational states of HF and DF, the scattering was predominantly backward. These v_f selective forward peaks were interpreted as manifestations of quantum mechanical (QM) resonances in reactive scattering, unlikely to be explained by classical mechanics.

SSDI 0301-0104(95)00360-6

These results prompted numerous theoretical studies [3–9] which, unsuccessfully, tried to reproduce the experimental findings. The discrepancies between experiment and theory were attributed to failures of the potential energy surface (PES), which, at that time, was believed to be strongly collinear [10,11].

The construction of new empirical [12] and semiempirical PES [13–16] allowed the qualitative reproduction of the DCS forward peaks in dynamical calculations, both quantum mechanical [16–18] and classical [12,19–22]. After these works, it became generally accepted that the relevant PES for this reaction has a bent transition state and a comparatively flat angular barrier to reaction. Nevertheless, the mentioned dynamical calculations on the new surfaces led to disagreements with other well established experimental results, such as product states distributions [1,2,23,24], reaction rate constants [25–27] or photoelectron spectra [28–31]. In addition, the fact that the DCS state selective forward peaks appear also in the quasi-classical trajectory results cast serious doubts on their interpretation as a manifestation of QM scattering resonances.

Recently, a new and totally ab initio PES for this reaction has been constructed by Stark and Werner (hereafter SW) [32–34]. Accurate QM calculations performed using this surface [35] could account for the electron photodetachment spectra of the FH_2^- ion obtained by Neumark and coworkers [28,29]. These experiments sample basically the transition state region of the potential energy surface. The asymptotic properties of reactive scattering on this PES have also been investigated. Quasi-classical trajectory (QCT) calculations on the SW PES [33,36] have revealed substantial accordance with the experimentally deduced CM differential cross sections and with the product state distributions reported by Lee and coworkers for $F+H_2$ and $F+D_2$ reactions [1,2], as well as with the recent and higher resolution data of Faubel et al. about $F+D_2$ [37–39]. In particular, the tendency from backwards to sideways peaking of $HF(v_f = 2)$ scattering with increasing E_{cm} and the state selective forward peaks in the DCS of $HF(v_f = 3)$ and $DF(v_f = 4)$, which had been succesively attributed to QM resonances, are obtained in these classical calculations.

A noteworthy difference between the experimentally deduced DCS for $F+H_2$ and those from QCT on the SW surface lies in the size of the forward peaks, the theoretical ones being smaller [33]. Accurate QM calculations of the $F+H_2(j_i = 0, 1, 2)$ on this PES carried out by Manolopoulos and coworkers [40] show that the forward peaks are substantially enhanced, especially for the initial rotational state $j_i = 0$. This was also the case in the calculations carried out on the semiempirical 6SEC PES, for which the comparison of QCT and exact QM differential cross sections for $F+H_2(j_i = 0, 1)$ [16,21] revealed that the classical forward peak was much smaller than in the quantal calculation.

More recently, the dymamics of the F+HD reaction has been thoroughly studied by QCT calculations carried out on the SW PES [41]. In order to compare with the molecular beam experimental results of Neumark et al. [2], simulations of the laboratory (LAB) angular distributions (AD) and time-of-flight (TOF) spectra were also performed. The results showed an excellent, quantitative, agreement in the case of the DF reaction channel. However, the comparison of the experimental and simulated LAB AD (the only available experimental information) in the case of the HF reaction channel, indicated strong discrepancies, which could be traced back to the absence of a forward peak in the QCT theoretical $HF(v_f = 3)$ CM DCS. This study proved the convenience, and, sometimes, the necessity, of carrying out the simulation of LAB data using the CM state resolved DCS in order to make a sound comparison, since some features are more clearly distinguished in the LAB frame.

Nevertheless, it is the $F+D_2$ reaction the one that have received more attention from the experimental point of view in the last years. The series of experiments reported by Faubel et al. [37–39,42] represent the state-of-the-art of the crossed molecular beam reactive scattering investigations not implying laser techniques, the resolution of the Göttingen molecular beam apparatus being several times larger than the one of the original work by Lee and coworkers [2]. Experiments have been carried out at many different collision energies covering a wide range of them. A clear and distinct identification of vibrational peaks has also allowed the determination of the v_f, j_f resolved CM DCS.

From the theoretical point of view, the accordance between the QCT calculations on the SW PES and the experimental data seems to be better for the $F+D_2$ than

for the other isotopic variants of the reaction [36]. In this case, the forward peaks deduced from the experiment [2] are satisfactorily reproduced and it is possible to simulate the recent high resolution TOF spectra [37,38] directly with the theoretical results. Furthermore, the QCT results at 144 meV predicted that both forward and backward scattering will increase with the D_2 rotational temperature. Measurements carried out at that energy and different stagnation pressure and temperatures of the nozzle, therefore, at several rotational temperatures of the D_2 beam [39], showed qualitative agreement with the QCT calculations. However, the magnitude of the backward and forward enhancement was definitively lower than the QCT theoretical predictions.

So far, the largest collision energy accesible for any isotopic variant of the $F+H_2$ in a crossed molecular beam experiment has been 140–144 meV. It remains to test the effect of a higher collision energy on the integral and differential reaction cross sections for these reactions. The preceding paper in this issue [43] presented the experimental integral and differential cross sections obtained at the collision energies of 180 and 240 meV, extracted by careful analysis and simulation of LAB measurements. Therefore, a theoretical investigation of this reaction at the same experimental conditions seems very timely. Taking that into account, we have performed extensive QCT calculations of the dynamics of the $F+D_2$ reaction on the SW PES for the range of experimental conditions of the molecular beam experiments of Ref. [43]. The calculations include state resolved integral and differential cross sections and reaction probabilities as a function of impact parameter at the two collision energies of the experiment. In order to compare more precisely with the measurements, we have undertaken the simulation of the primary experimental data, i.e. angular distributions and time-of-flight spectra in the laboratory frame. The QCT results are analyzed in terms of the detailed dynamical mechanism.

2. Method

The general method of calculation of quasiclassical trajectories is the same one as used in previous works. It is described more extensively in Refs. [44,45] (see also Ref. [46]) and only the particular details relevant to the present work will be given here.

The calculations on the ab initio SW potential energy surface have been performed for the $F+D_2(v_i = 0, j_i = 0, 1, 2)$ reaction at collision energies of 180.0 meV (4.15 kcal mol^{-1}) and 240.0 meV (5.53 kcal mol^{-1}), corresponding to the average collision energies of the molecular beam experiments of Faubel et al. [43]. Batches of 60 000 trajectories have been calculated at each energy and initial rotational quantum number j_i.

The major change with respect to previous studies has been the quantization of the initial rotational angular momentum of the D_2 molecules. Until now, the square of the rotational angular momentum was equated to $j_i(j_i+1)\hbar^2$; thus, for $j_i = 0$ the molecules had absolutely no rotational motion. However, Azriel et al. [47], in a very recent article, pointed out that the use of the semiclassical quantization resulting of replacing $j_i(j_i+1)\hbar^2$ by $(j_i+1/2)^2\hbar^2$ (Langer correction [48]), produces a somewhat better agreement with exact QM calculations carried out in the same PES. In fact, we had observed that the addition of a "residual" rotation to $j_i = 0$ improves the agreement not only with QM calculations, but also with the experimental results, and in the case of the SW PES more significantly than in the case of any other PES. Therefore, in this study we have adopted such quantization, which, in fact, is only important for the D_2 in $j_i = 0$. The results are practically insensitive to whether j_i was kept fixed for all the trajectories, or whether j_i was randomly (uniformly) varied in the range $[j_i - 1/2, j_i + 1/2]$ for every individual trajectory. In addition, the choice of this quantization for the assignments of products' quantum numbers had no noticeable influence (within the statistical uncertainties) on the product state distribution. The assignment is done by equating the classical DF molecule rotational angular momentum to $(j_f + 1/2)\hbar$. With the (real) j_f value so obtained, the vibrational quantum number v_f is found by equating the internal energy of the outgoing molecule to a rovibrational Dunham expansion containing 20 terms (fourth power in $v_f + \frac{1}{2}$ and third power in $(j_f + 1/2)^2$) calculated by fitting the rovibrational energies given by the asymptotic diatomic limits of the SW PES. The values of v_f and j_f found in this way are then rounded to the nearest integer.

The vibrationally state resolved differential cross sections, $d^2\sigma/d\omega$, were calculated by the method of

moments expansion in Legendre polynomials (see Refs. [45,46]). The Smirnov–Kolmogorov test comparing the cumulative probability distributions was used to decide when to truncate the series. Significance levels higher than 95% could be achieved using 8–12 Legendre moments, ensuring a very good convergence such that the inclusion of more terms does not produce any significant change. Special care was paid to the analysis of particular structures in the differential cross sections which remain unaffected when the number of Legendre moments are changed in ±2. The error bars, calculated as in Ref. [45], correspond to plus/minus one standard deviation. The reaction probabilities as a function of the impact parameter (opacity functions) were also calculated using the method of moments expansion in Legendre polynomials as described in Ref. [45].

The simulation of the TOF spectra and of the LAB AD of scattered DF molecules is carried out by transforming the theoretical CM v_f,j_f DCS into the LAB system using exactly the same method described in the preceding paper [43] and in Ref. [41]. It should be stressed that no adjustable parameters have been used in these simulations.

When comparing with the experimental results, both the CM DCS and the LAB TOF and AD are appropriately weighted using the experimental initial rotational distribution of the D_2 molecules (see Table 2 of Ref. [43]).

3. Results and discussion

Table 1 summarizes the calculated vibrationally resolved and total integral cross sections on the SW PES at the two collision energies and initial rotational quantum numbers j_i = 0–2. None of these values are corrected for the fact that there are two competing potential surfaces that correlate with the ground state reagents (although only one of these states correlates with the products' electronic ground state). The present calculations, purely adiabatic, ignore absolutely the existence of this upper PES and no multisurface factor is included (see Ref. [36] and references therein).

From Table 1 it can be seen that, at the two collision energies and the initial j_i studied in this work, the total reactive cross section increases with collision energy for all initial D_2 rotational states here considered, although for j_i = 1 and j_i = 2 it does more slowly. From the energetics point of view, it is evident that initial rotation is more effective than translation in promoting the reaction (the energy difference between the j_i = 2 and j_i = 0 levels is just 22 meV). The comparison of the present results with those calculated at lower collision energies [36] on the same PES, shows that as E_{cm} increases the augment of $\sigma_R(E_{cm})$ tend to be less important. In any case, and for j_i = 0–2, the $\sigma_R(E_{cm})$ grows monotonically with E_{cm}. This is in contrast with the results of recent QCT total reaction cross section calculations carried out on the 6SEC PES in a wide range of collision energies [49], for j_i = 0–4, that indicate that for energies above 4 kcal mol^{-1} ($\approx$ 170 meV) the $\sigma_R(E_{cm})$ levels off [49].

The branching ratios into the different product vibrational states, defined as $\rho = \sigma_R(v_f)/\sigma_R(v_f = 3)$ (shown in parentheses in Table 1), do not change much with collision energy for v_f = 2–4, whereas for v_f = 1, 2 increase appreciably. In general, translational energy tends to favour low v_f, whereas the initial rotation clearly favors v_f = 4, and in a lesser extend v_f = 3. In fact, for collision energies above 140 meV, the increase in the total cross section with j_i goes to v_f = 3 and v_f = 4 exclusively. As such, the branching ratios into v_f = 0–2 decrease as initial j_i increase, and just the opposite holds for the one into v_f = 4. Thus, when going from j_i = 0 to j_i = 2, $\sigma_R(v_f = 4)$ triples.

The vibrational branching ratios at each energy can be compared with those extracted from the analysis of the experimental data [43]. In the two cases, the experimental and theoretical $\rho(v_f)$ are in a quite good agreement. At 180 meV only, the one into v_f = 2 seems to be somewhat overestimated by the calculations. At 240 meV, the experiment yields more v_f = 4 and less v_f = 2 than those predicted by the QCT calculations.

Table 2 displays the fraction of total energy released as translation, rotation and vibration of the products. In all the cases the largest fraction of the available energy appears as vibration of the DF product. This fraction decreases with the collision energy but increases substantially with the initial j_i. The opposite happens with $\langle f_T \rangle$. The fraction into rotation is the lowest in all cases, but it seems to increase with both E_{cm} and j_i. In general, the results averaged on the initial j_i states agree well with the experimental ones [43], which are also shown in Table 2. The fraction into translational

Table 1
Integral cross sections $\sigma_R(Å^2)$ for the production of DF(v_f) at the collision energies of 180 and 240 meV. Values in parentheses are the branching ratios defined as $\sigma_R(v_f)/\sigma_R(v_f = 3)$

	Method	$v_f = 0$	$v_f = 1$	$v_f = 2$	$v_f = 3$	$v_f = 4$	$v_f = 5$	all v_f
$E_{cm} = 180$ meV	QCT($j_i = 0$)	0.08 (0.05)	1.16 (0.69)	2.41 (1.43)	1.68 (1.0)	0.40 (0.24)	–	5.73
	QCT($j_i = 1$)	0.04 (0.02)	1.00 (0.47)	2.45 (1.14)	2.15 (1.0)	0.68 (0.32)	–	6.32
	QCT($j_i = 2$)	0.04 (0.01)	0.78 (0.29)	2.36 (0.88)	2.69 (1.0)	1.17 (0.43)	–	7.04
	QCT(o-D_2) [a]	0.06 (0.03)	1.03 (0.51)	2.40 (1.19)	2.02 (1.0)	0.65 (0.32)	–	6.17
	Experiment [b]	(0.02)	(0.45)	(0.91)	(1.0)	(0.33)	–	
$E_{cm} = 240$ meV	QCT($j_i = 0$)	0.25 (0.14)	1.47 (0.83)	2.63 (1.49)	1.77 (1.0)	0.41 (0.23)	0.00 (0.00)	6.53
	QCT($j_i = 1$)	0.18 (0.09)	1.32 (0.67)	2.67 (1.35)	1.98 (1.0)	0.63 (0.32)	0.02 (0.01)	6.80
	QCT($j_i = 2$)	0.13 (0.05)	1.14 (0.47)	2.69 (1.10)	2.45 (1.0)	0.95 (0.39)	0.03 (0.01)	7.39
	QCT(o-D_2) [c]	0.18 (0.08)	1.28 (0.59)	2.67 (1.24)	2.16 (1.0)	0.72 (0.33)	0.02 (0.01)	7.03
	Experiment [b]	(0.05)	(0.53)	(0.96)	(1.0)	(0.40)	–	

[a] T_{rot}= 110 K. o-D_2 is a gas mixture of 90% ortho-D_2 and 10% para-D_2. Rotational population: 61% $j_i = 0$; 10% $j_i = 1$; 29% $j_i = 2$.
[b] Ref. [43], preceding paper in this issue. [c] T_{rot} = 195 K. o-D_2 is a gas mixture of 90% ortho-D_2 and 10% para-D_2. Rotational population: 37% $j_i = 0$; 8% $j_i = 1$; 55% $j_i = 2$.

Table 2
Average values of the fraction of total energy released as translation $\langle f_T \rangle$, rotation $\langle f_R \rangle$ and vibration $\langle f_V \rangle$. The average final rotational number is also shown for each vibrational state

	E_{cm} = 180 meV					E_{cm} = 240 meV				
	$j_i = 0$	$j_i = 1$	$j_i = 2$	o-D_2 [a]	Expt. [b]	$j_i = 0$	$j_i = 1$	$j_i = 2$	o-D_2 [c]	Expt. [b]
$\langle f_T \rangle$	0.383	0.338	0.293	0.352	0.318	0.400	0.366	0.323	0.355	0.322
$\langle f_R \rangle$	0.063	0.074	0.085	0.070	0.092	0.084	0.096	0.109	0.099	0.114
$\langle f_V \rangle$	0.554	0.587	0.623	0.577	0.590	0.516	0.539	0.567	0.546	0.564
$\langle j_f \rangle_{v_f=0}$	8.69	9.78	10.58	9.35	13.0	9.44	10.84	11.43	10.65	13.9
$\langle j_f \rangle_{v_f=1}$	7.89	10.54	12.07	9.37	12.6	9.83	11.74	13.48	12.00	14.4
$\langle j_f \rangle_{v_f=2}$	8.66	10.01	11.56	9.64	10.8	10.41	11.38	12.92	11.87	12.4
$\langle j_f \rangle_{v_f=3}$	8.68	8.67	9.42	8.89	9.9	10.18	10.31	10.93	10.60	11.3
$\langle j_f \rangle_{v_f=4}$	7.23	6.49	6.36	6.90	5.4	7.06	7.18	7.44	7.28	6.6

[a] T_{rot} = 110 K. o-D_2 is a gas mixture of 90% ortho-D_2 and 10% para-D_2. Rotational population: 61% $j_i = 0$; 10% $j_i = 1$; 29% $j_i = 2$.
[c] T_{rot} = 195 K. o-D_2 is a gas mixture of 90% ortho-D_2 and 10% para-D_2. Rotational population: 37% $j_i = 0$; 8% $j_i = 1$; 55% $j_i = 2$.
[b] Ref. [43], preceding paper in this issue.

energy deduced from the experiment is slightly smaller than the theoretical value at the two collision energies, whereas $\langle f_R \rangle$ is somewhat larger. The observed trends with collision energy are very well accounted for by the QCT calculations. Table 2 also contains the mean values of the final DF rotational state $\langle j_f \rangle$ for each final v_f state. Except for $v_f = 4$, the average $\langle j_f \rangle_{v_f}$ increase with both E_{cm} and initial j_i. Thus, the present calculations anticipate a hotter rotational distribution as the D_2 rotational temperature increases.

The rotational j_f state distributions for each product vibrational v_f state, at the two collision energies of this study, are presented in Fig. 1. The results are averaged on the initial j_i distribution of the D_2 molecules, and, therefore, are directly comparable to those of Fig. 8 of Ref. [43]. Overall, the QCT results predict quite well the main features observed in the experimental state distributions. The maxima of the QCT rotational state distributions for each v_f are, in general, slightly shifted towards lower j_f with respect to the experimental ones. The calculated distributions are, however, broader, especially for $v_f = 2$ and for $v_f = 4$. In the latter case, the QCT calculations yield a hotter rotational distribution. The resulting mean values of j_f from both the present

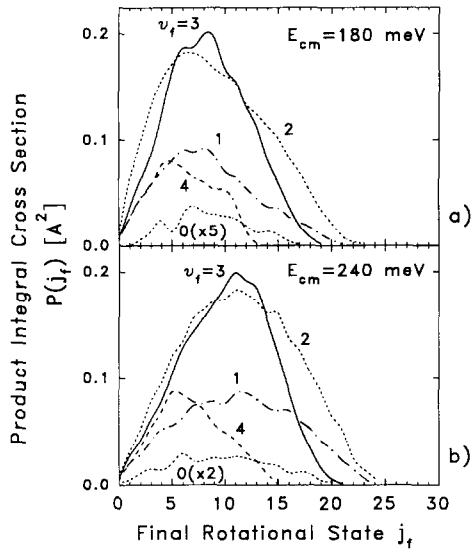

Fig. 1. Calculated rotational distributions for individual vibrational states of the DF product. Upper panel: collision energy E_{cm} = 180 meV; lower panel: E_{cm} = 240 meV. In the two cases the state distributions are weighted on initial D_2 j_i states according to the experiments and the results are directly comparable with Fig. 8 of the preceding paper [43].

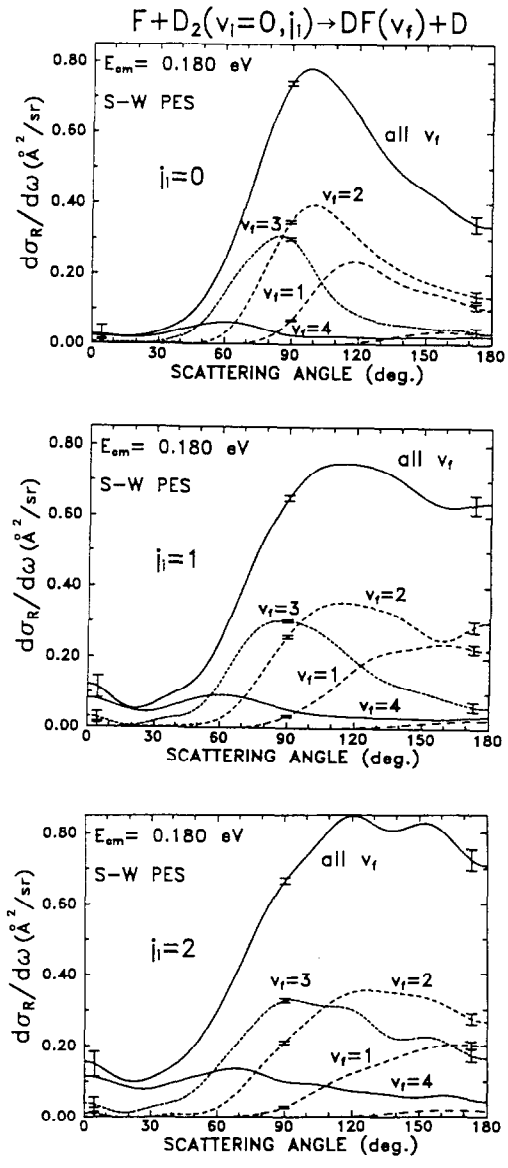

Fig. 2. Theoretical center of mass differential cross sections for the $F+D_2(v_i = 0, j_i = 0,1,2)$ reaction resolved into the final vibrational states of the DF product, v_f, at a collision energy of 180 meV and for the indicated initial quantum numbers j_i. Error bars correspond to one standard deviation of the fits.

calculation and the experiment are shown in Table 2. The experimental values $\langle j_f \rangle_{v_f}$ at the two energies are systematically larger for all cases, except for $v_f = 4$, for which the QCT results predict a higher value of $\langle j_f \rangle_{v_f=4}$.

Figs. 2 and 3 display the CM v_f-resolved DCS at 180 and 240 meV respectively, for the D_2 initial j_i = 0,1 and 2 rotational states. The general shape and the evolution with j_i are very similar for the two energies and also similar to the ones calculated at 144 meV of Ref. [36]. It must be recalled that in that work, the $j_i(j_i+1)\hbar^2$ quantization was used, and, thus, for $j_i = 0$, the molecules were initially strictly rotationless. The most salient features are the evolution of backward and forward scattering with j_i. For $j_i = 0$, the scattering is mainly sideways, extending towards 180 degrees. As j_i increases, the backward scattering is recovered. On the other hand, the forward peak clearly grows with j_i, especially when going from $j_i = 0$ to $j_i = 1$. As the collision energy increases for a given j_i, the DCS are broader, the forward component augments, and the peaks of the DCS shift towards lower angles. In general, the roles of collision energy and initial j_i seem to affect the DCS in a similar way, although the effect of the initial rotation is always more important. The main contribution to the forward peak comes from $v_f = 4$, however, the participation of $v_f = 3$, especially as the collision energy increases, is not negligible. The $v_f = 3$ DCS is less affected by both the initial j_i and

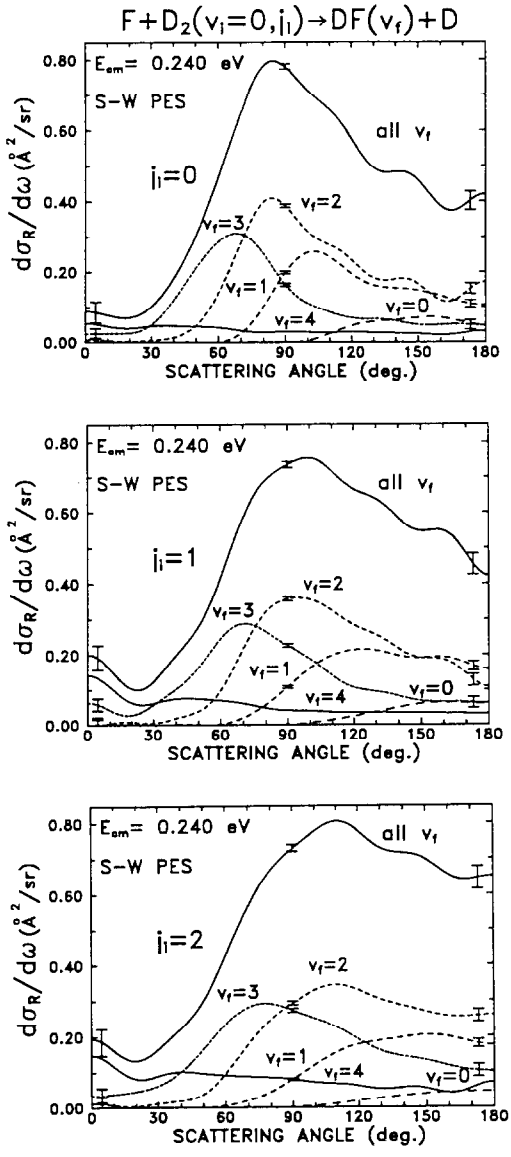

Fig. 3. Same as Fig. 2 but for the collision energy 240 meV.

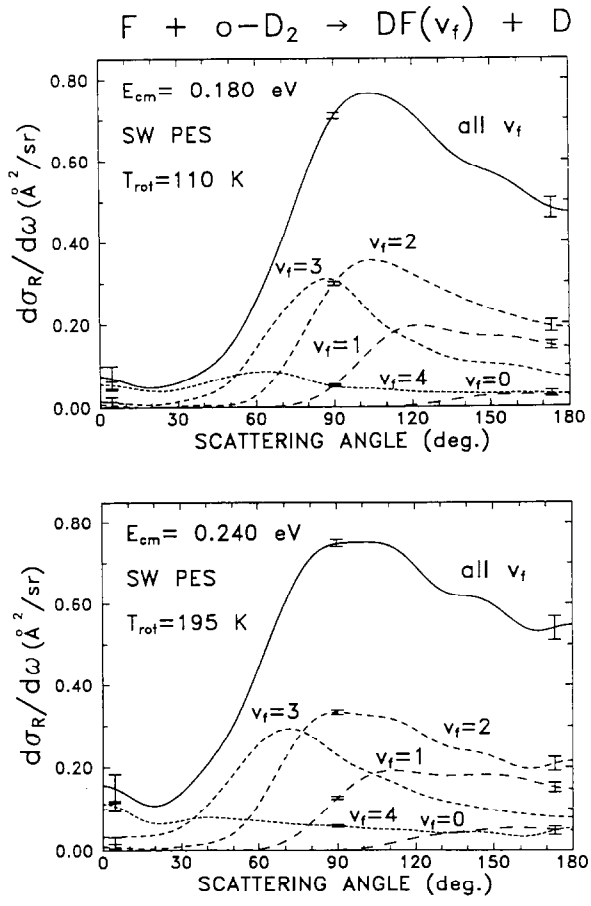

Fig. 4. Vibrational state resolved CM differential cross sections weighted for an initial population of the D_2 rotational states, j_i, according to the conditions of the experiment, shown in Fig. 6 of Ref. [43].

the collision energy than the other state resolved DCS, but as j_i increases, for a given E_{cm}, the backward tail of $v_f = 3$ becomes larger. The forward component of the $v_f = 4$ scattering, for a given j_i, also increases with E_{cm}, whilst the opposite tendency affects the broad peak at the CM scattering angle 60°. The $v_f = 1, 2$ DF scattering, which is the main contribution to the total DCS in the backward hemisphere, clearly shifts towards 180° as j_i increases, and the corresponding state resolved DCS change from being sideways to essentially backward at the two energies of this work, and at 144 meV [36].

Fig. 4 displays v_f-resolved DCS at the two collision energies, averaged on initial j_i according to the indicated rotational temperatures which correspond to the ones estimated for the experiment presented in the preceding paper of this issue, and, therefore, can be directly compared with those of Fig. 6 of that paper [43]. Although there is a general qualitative agreement, there are noticeable differences. At the two energies, the QCT calculations certainly underestimate the backward scattering and the magnitude of the forward peak. Since the participation of $D_2(j_i = 0)$ is the main one, it follows that the QCT results for $j_i = 0$

predict too little backward and forward scattering. Indeed, the agreement would markedly improve if the QCT $j_i = 0$ DCS is substituted by the $j_i = 1$ or $j_i = 2$ DCS. Therefore, the use of a $j_i + 1/2$ semiclassical quantization is not sufficient to reconcile the present calculations on the SW PES with the experimental results. Whereas, at the two E_{cm}, the $v_f = 3$ DCS is the one in better agreement with their experimental counterparts, the QCT $v_f = 2$ DCS is shifted towards lower angles and is missing some backward scattering. The experimentally deduced DCS for $v_f = 1$ at the two energies are more confined into backward angles than the corresponding QCT ones, and, in the case of 240 meV, the calculations underestimate its magnitude. Interestingly, the experimentally deduced DCS summed on all v_f states shows some undulations that correspond to the maxima of each v_f resolved DCS. The theoretical v_f resolved DCS are sensibly less separated in the angular range and, consequently, the total DCS is quite structureless.

The vibrational specificity of the forward scattering deserves some consideration. The forward peak, whose magnitude is underestimated in the QCT calculations, proceeds from $v_f = 4$ mainly, but it also has contribution from $v_f = 3$, especially at 240 meV. However, the experimental results seem to indicate that all the forward scattering is caused by $v_f = 4$ solely, although, as the energy increases, the $v_f = 3$ DCS tends to extend towards smaller CM angles. Since no TOF has been measured at LAB angles below 9° in the LAB system, the existence of a $v_f = 3$ forward peak cannot be ruled out, as discussed in the previous paper [43]. However, the hypothetical $v_f = 3$ forward scattering would have to be confined into a quite narrow range of CM angles (0°–30°), to be compatible with the present experimental results. The experimental TOF spectra indicate that, at $E_{cm} = 180$ meV, the $v_f = 3$ scattering decreases monotonically until a CM angle of 30° (the lowest one experimentally accessible for this state) becoming at this angle almost null. A subsequent rise of the $v_f = 3$ CM scattering would not be detectable by the present experiments.

Fig. 5 just shows the simulation of a series of TOF at the indicated LAB angles for the two energies here considered. All the QCT TOF simulated spectra (solid line) have been scaled to the experimental ones (dots) using the same factor. Specifically, at $E_{cm} = 180$ meV, the simulated QCT one at $\Theta_{lab} = 9.5°$ is clearly at variance with the experimental one. The predicted magnitude is about 5.4 times smaller than the experimental one. If, for clarity purposes, the QCT TOF is scaled to the experimental TOF peak (dashed line in Fig. 5), it becomes clear that the QCT predicted ratio of $(v_f = 3)/(v_f = 4)$ is much larger than the experimental one at this LAB angle. Therefore, a flat $v_f = 3$ CM forward tail of a *relative* magnitude with respect the $v_f = 4$ forward scattering, as the one given by the QCT calculations would not be compatible with the experimental results.

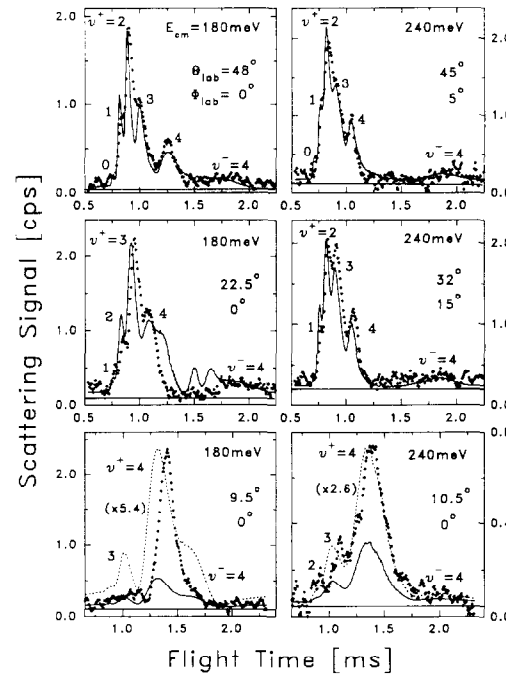

Fig. 5. Comparison of experimental (points) time-of-flight spectra and simulated spectra (line) using the present QCT v_f,j_f state resolved DCS at the collision energies and LAB angles indicated in each figure. The scaling factor between experimental and simulated TOF data is the same for all spectra shown here and agrees with the factor obtained for the LAB AD (see below). At the two lowest angles, $\Theta_{lab} = 9.5°$ at $E_{cm} = 180$ meV, and $\Theta_{lab} = 10.5°$ at 240 meV, the additional dotted line shows the QCT simulated TOF spectra scaled with the additional factor indicated in parenthesis, in order to match the height of the experimental $v_f = 4$ peak. The peaks are labeled with the corresponding final vibrational state of the DF product. The +/− subindices are used to distinguish between scattering to the right/left of the relative velocity leading to fast/slow molecules.

Recent accurate QM calculations by Manolopoulos and coworkers for the F+H_2 reaction on the same PES

[40] produce a forward tail in $v_f = 2$ (equivalent to $v_f = 3$ in the F+D_2 reaction) of a relative size compared to the $v_f = 3$ (equivalent to DF($v_f = 4$)) much bigger than the one obtained by QCT calculations. In fact, this forward $v_f = 2$ scattering seems to have its origin in a resonance in the exit channel. Nonetheless, the simulation of the LAB TOF of Lee and coworkers with the QM DCS data [40] allows to establish that such a $v_f = 2$ tail is likely to be incompatible with the experimental results [1].

In addition, the peak corresponding to the fast $v_f = 4$ in the QCT simulation at $\Theta_{lab} = 9.5°$ is displaced towards shorter times with respect to the experimental one, thus, indicating that the experimental $v_f = 4$ scattering is rotationally hotter than theoretically predicted. At $E_{cm} = 240$ meV there is a better agreement between the QCT simulated TOF and the experimental one at $\Theta_{lab} = 10.5°$, when both are normalized to the $v_f = 4$ peak (dashed line). However, the relative magnitude is still a factor of about 2.6 less than the experiment. At this energy the experimental CM $v_f = 3$ scattering is broader, and it shows up as a fast small peak in the TOF spectrum.

The TOF at $\Theta_{lab} = 22.5°$ and $E_{col} = 180$ meV corresponds to the CM region 75–85°, and some interesting conclusions can be drawn from the comparison of experiment and simulation. The magnitude of the QCT $v_f = 3$ peak is in very good agreement with the experimental one, whereas the $v_f = 2$ scattering is overestimated in the simulated TOF spectrum. This is easily explainable in terms of the v_f resolved DCS of Fig. 4 of the present paper and Fig. 6 of the preceding paper. In addition, the experimental $v_f = 3$ is hotter than the QCT one. The opposite seems to happen for the $v_f = 4$ scattering, and this fact has a noticeable effect in the LAB AD (see below). The TOF spectrum at $\Theta_{lab} = 32°$ and $\Phi_{lab} = 15°$ and 240 meV, very close to the direction of the centroid (see Fig. 2 of the preceding paper), samples the CM sideways scattering ($\approx 80°$). The $v_f = 1$ and $v_f = 4$ experimental peaks are smaller and bigger, respectively, than the corresponding QCT ones, as can be expected from the v_f resolved DCS. The other two QCT TOF at each energy, portrayed in Fig. 5 (which, depending on the v_f state, correspond to the CM angles 130–150°), are, in fairly good agreement with the experimental results. In general, this good agreement persists at higher angles, at least in the widths and relative heights of the different peaks.

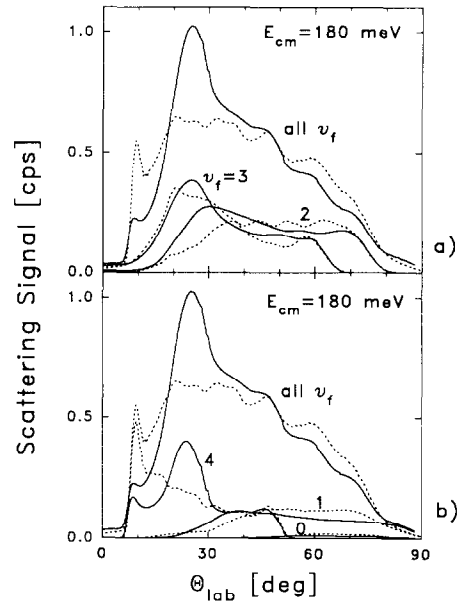

Fig. 6. LAB angular distributions of product flux at 180 meV. Dashed line: experimental results (as described in the preceding paper of this issue); solid line: simulation carried out with the present QCT results. For clarity the upper panel shows the total LAB AD and the contributions from $v_f = 2, 3$, only. The lower panel represents the total LAB AD and the contributions from $v_f = 0, 1, 4$.

It also seems interesting to compare the experimental LAB frame angular distributions (LAB AD), shown in Fig. 5 of the preceding paper, with the simulations using the present QCT results. Figs. 6 and 7 show such comparison between QCT simulated and experimental "in plane" ($\Phi_{lab} = 0$) LAB AD at $E_{cm} =$ 180 and 240 meV, respectively. The analysis of the v_f contributions to the total LAB AD are also represented in these figures. The QCT simulated LAB AD at 180 meV presents a broad peak at $\Theta_{lab} = 22$–30°, which is clearly at variance with the experimental data, that comes mainly from $v_f = 2$ and $v_f = 4$. In addition, the magnitude of the peak at $\Theta_{lab} = 8$–10°, caused by the $v_f = 4$ CM forward peak, is significantly smaller in the case of QCT. For Θ_{lab} above 40°, there is a fairly good agreement between the two curves. At 240 meV (Fig. 7) the discrepancies are less important, although, the QCT calculations still predict excessive scattering at Θ_{lab} between 30°–50°. The analysis of LAB AD in the contributions from every v_f state reveals a good

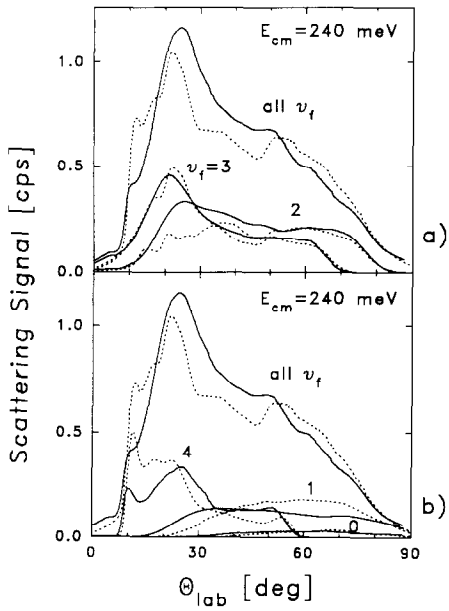

Fig. 7. Same as Fig. 6, but for the collision energy E_{cm} =240 meV.

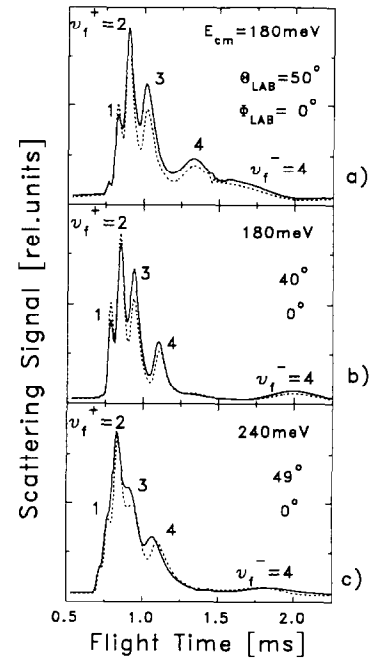

Fig. 8. Simulations of TOF spectra at E_{cm} = 180 meV (a),(b), and at E_{cm} = 240 meV (c) for different D_2 initial rotational state population. Solid line: high rotational temperatures [T_{rot} = 180 K for panel (a) and (b); T_{rot} = 250 K in (c)]. Dashed line: low rotational temperature [T_{rot} = 110 K for panel (a) and (b); T_{rot} = 165 K in (c)]. The results are to be compared with those of Fig. 7 of the preceding paper in this issue.

agreement between experimental and calculated v_f = 1, and, especially, v_f = 3 LAB AD, at the two collision energies here considered. In contrast, as already mentioned, the v_f = 4 experimental and QCT LAB AD are very different, more than the mere inspection of the corresponding CM v_f seems to indicate.

A detailed analysis of that broad peak in the QCT simulated AD shows that it results from v_f = 4, rotationally hot (j_f = 8–11) scattering, which, in fact, produces the broad peak centered at 60° in the CM v_f = 4 DCS. This is also corroborated by the TOF spectrum at 180 meV and Θ_{lab} = 22.5° (Fig. 5), as discussed above. Furthermore, this peak mainly originates by scattering from the initial j_i = 0 state. This is a clear example of how relatively minor features in the CM frame might have important consequences in the LAB frame observables. The analysis of the forward scattering (which appears in the range of Θ_{lab} = 7–12°) shows that it is rotationally considerably hotter than the theoretical prediction. On the other hand, the very noticeable discrepancy between experimental and QCT CM backward scattering is only manifest in the LAB AD by a slightly larger amount of LAB flux in the experimental case for Θ_{lab} between 55° and 80°.

The shape and evolution of the QCT v_f-resolved DCS with the initial rotational state, already shown in Figs. 2 and 3, suggest that, as the rotational temperature of the D_2 reagent increases (therefore, implying larger contributions of j_i = 1,2), the experimentally determined DCS would tend to become more backward peaked, especially for v_f = 1,2. And the forward peak in v_f = 4 should be more prominent. The experiments carried out at 140 meV, at different T_{rot}, showed that this was, in fact, the observed tendency [39]. However, this effect was sensibly smaller than predicted by the QCT calculations [36]. In the preceding paper [43] the effect of the rotational temperature of the D_2 reagent has been also studied at 180 and 240 meV collision energy, at LAB angles correponding to high CM angles (see Fig. 7 of the preceding paper). The experimental findings are that the cross section grows significantly for the v_f = 3,4 product states. Fig. 8 represents the simulation of the TOF spectra shown in Fig. 7 of the preceding paper [43], using the QCT v_f, j_f DCS. Despite of the clear differences between QCT simulated and experimental TOF spectra

for both rotationally "cold" (dashed line) and "hot" (solid line) results, the tendency as T_{rot} increases is very similar. The QCT simulations at 180 meV (panels (*a*) and (*b*)) indicate that the $v_f = 3$ scattering increases substantially at these angles (which roughly correspond to 150°–180° in the CM system), in excellent agreement with the experimental findings. At this energy, there is also a noticeable increase in the $v_f = 4$ scattering (170°–180° in the CM), which is, however, slightly smaller than the experimental one. On the other hand, the QCT simulations indicate an increment in the $v_f = 1, 2$ scattering (140°–155° in the CM), which does not seem to occur in the experimental results.

At 240 meV, the comparison between the QCT and experimental TOF spectra at the two T_{rot} yields a very good agreement. Despite of the fact that there is a smaller change in the rotational populations as compared with 180 meV, there is a very strong enhancement in the $v_f = 3$ and $v_f = 4$ scattering at that LAB angle (which also corresponds to backward CM angles). The increase in the $v_f = 3$ scattering is also found in the classical simulation; for $v_f = 4$, the QCT calculations predict a shift in the peak towards faster velocities when T_{rot} increases, which is also found in the experiment, however, the signal increase in the latter case is substantially larger than in the QCT case. The consequence is that the actual enhancement of backward scattering in $v_f = 4$ as j_i increases seems to be, in fact, larger than the one predicted by the QCT results.

In order to gain more insight into the dynamics of this reaction, we have calculated the reaction probability as a function of the impact parameter, i.e. the opacity function $P(b)$, at the two collision energies here studied. Fig. 9 shows the results at 180 meV and initial $j_i = 0$–2. In all cases, and at a first glance, the shapes of the opacity functions summed on all final states, resemble those of a simple line-of-centers model, i.e. reaction probability equal to one up to a given maximum impact parameter. This is not surprising taking into account the very flat bending potential of this PES. At an energy high enough to surmount the barrier, the cone of acceptance comprises almost all space. The maximum impact parameter, b_{max}, which at these E_{cm} is really governed by the centrifugal barrier, increases noticeably with initial j_i. This effect was also found in the other isotopic variants of this reaction [41]. In all

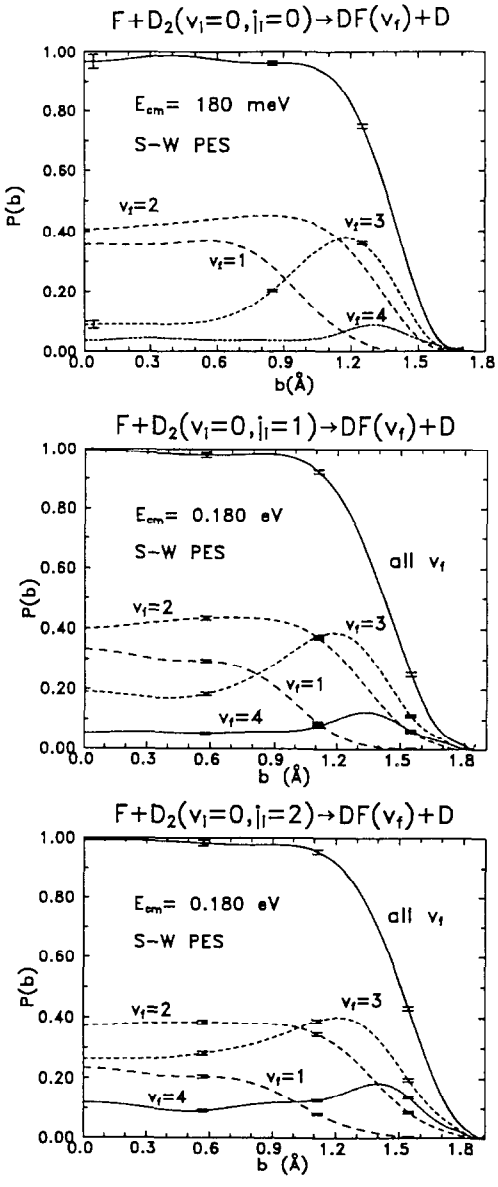

Fig. 9. Reaction probability as a function of the impact parameter (opacity function) for E_{cm} = 180 meV and $j_i = 0$ (top), $j_i = 1$ (middle), and $j_i = 2$ (bottom).

cases, it was found that rotation of the diatom helps to find the minimum barrier as the F atom approaches with very low radial energy (corresponding to high impact parameters). The inspection of the v_f-resolved $P(b)$ indicates that the contributions from high impact parameter mainly go to the highest v_f states. In

particular, a detailed analysis shows that the $v_f = 4$ forward peak shows that is just made of contributions from a very limited range of the highest impact parameters, or, in QM terms, of very few total angular momentum J partial waves, in a extraordinary similitude with the QM results for the analysis of the $v_f = 3$ forward peak of the F+H_2 reaction [40].

The comparison of experiment and QCT on this PES corroborates a shortcoming of QCT calculations; namely, that the forward peak produced by $j_i = 0$ is clearly underestimated. This is evident from the comparison of QCT and experimental results in both the CM and LAB frame. Accurate QM calculations on this and other PES for the F+H_2 reaction [40] show that tunneling for high orbital angular momenta is decisive in the building up of the forward peak, especially for $j_i = 0$. Similar behaviour was found when QM and QCT results on the 6SEC PES were compared [16,21]. Therefore, although by itself the HF($v_f = 3$) forward scattering is not a quantum effect since it is also found in the classical calculations, it is evident that is greatly enhanced in the QM calculations. If the forward peak is, at least, partly caused by tunneling through the centrifugal barrier, one should expect substantially lower forward peaks for the F+D_2 reaction at similar collision energies, which seems to be case. On the other hand, the comparison of the QCT results for the F+H_2 and F+D_2 on the same PES [20,33,36] shows that the magnitude of the forward peak at a given energy is greater for the first isotopic variant, and that the threshold for its appearance is smaller for the F+H_2 reaction. The different zero point energies for the two reactions might explain this fact, although in the transition state the vibration of the diatom is still practically unaltered.

The addition of one or two rotational quanta in the H_2, D_2 or HD molecules causes a substantial increase in the forward peak in the QCT calculations carried out on this PES. This is also reflected in the opacity functions shown in Fig. 9; as j_i increases, b_{max} also grows, and the larger angular momenta produce an increased forward peak. The rotational motion of the diatom seems to couple very efficiently with the motion on the barrier, helping to overcome it, and thus allowing higher b's to participate in the reaction. However, in the QM calculations it is not so clear that a larger j_i will produce more HF($v_f = 3$) forward scattering [40]. In general terms, the agreement between the magnitude of the QCT and QM forward peaks improves with j_i.

In the case of the present study, as mentioned before, the agreement would be much better if the QCT $j_i = 0$ DCS were substituted by those of $j_i = 1, 2$. The inclusion of the $(j_i + 1/2)$ quantization, and thus a "residual" rotational motion when $j_i = 0$, plays a minor role in the DF($v_f = 4$) forward scattering. The main consequence is that a better accordance between experiment and QCT calculations can be expected as T_{rot} increases, and this seems to be the case [2,36,39].

Fig. 10 portrays the opacity functions at 240 meV. The comparison with those at 180 meV shows that, for a given j_i, the maximum impact parameter also grows with collision energy. Accordingly, one might expect more forward scattering as the energy increases. Whereas this is the case in the QCT calculations, it is not so clear experimentally. It is also important to remember that the fraction of molecules in $j_i = 0$ at this energy is $\approx$ 40%, against $\approx$61% at E_{cm} = 180 meV. At E_{cm} = 240 meV, the maximum impact parameter increases very little with j_i, and the increase in the contribution from $b > 1.5$ Å, when going from $j_i = 0$ to $j_i = 2$ is small compared with the one occurring at 180 meV. It is worth noticing the increase in the high impact parameter contribution to $v_f = 3$, which seems to cause a growth in the $v_f = 3$ forward scattering.

The fact that larger impact parameters can lead to reaction as E_{cm} and the initial j_i go up implies higher j_f, and, therefore, a higher fraction of the available energy for the products channelling into rotation. The effect of the increase of E_{cm} in $\langle f_R \rangle$ and in the $\langle j_f \rangle_{v_f}$ is also observed experimentally.

Interestingly, saturation of the $P(b)$ seems to occur at low b, irrespective the initial j_i considered, and at the two collision energies. A more detailed inspection of the opacity functions for $j_i = 0$, shows that, for the lowest impact parameters, between 0 and 0.4 Å, the probability is slightly, but significantly, below 1, whereas the ones for $j_i = 1, 2$ are (within the statistical uncertainty) equal to 1. A careful analysis of reactive and non-reactive trayectories in this range of impact parameters and $j_i = 0$ showed that the orientations corresponding to an angle of attack close to 90° are especially unfavourable in producing reaction. These trajectories hit the repulsive wall in the PES between the two wells corresponding to the reactive ends of the D_2 molecule (see, for instance, Fig. 15 of

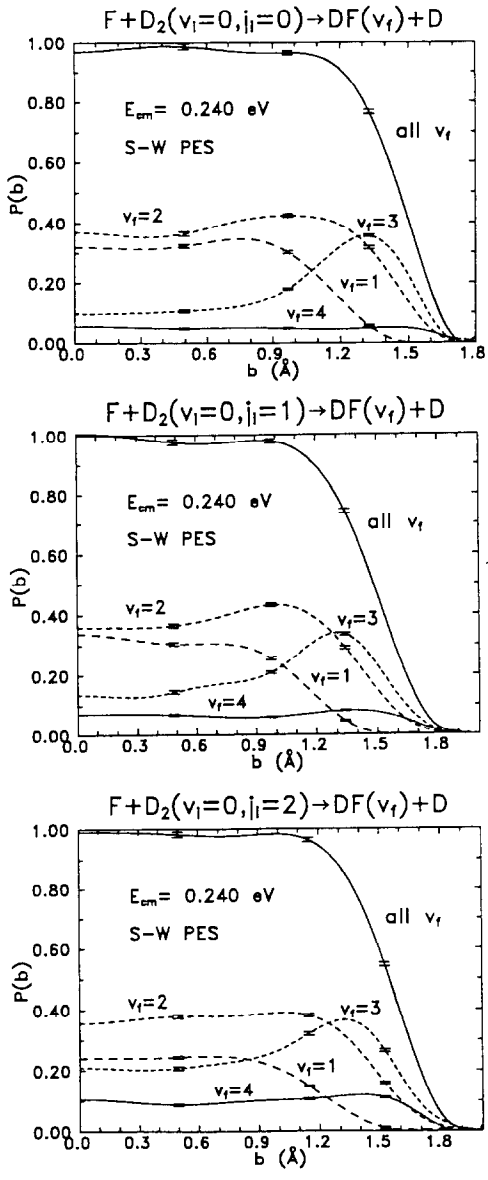

Fig. 10. As Fig. 9, but for E_{cm} = 240 meV.

Ref. [41]) and rebound, causing rotational excitation but no reaction. As the impact parameter increases, the angular motion caused by the orbital momentum helps to avoid the frontal collisions with the sideways wall, and $P(b)$ becomes equal to one. Initial rotation produces the same effect, even for small values of b. Therefore, the $P(b)$ for j_i = 1, 2 are saturated from b = 0 up to b values where the centrifugal barrier becomes important. This orientation dependent effect serves to explain the depletion of backward scattering for j_i = 0 in part. In addition to this, it is also found that, as j_i increases, larger impact parameters participate in the backward scattering ($\theta_{cm} > 150°$). Whereas the depletion of backward scattering for j_i = 0 seems to be overestimated in the QCT calculations (see Fig. 4 of the present paper and Fig. 6 of the preceding paper [43]), the simulation of the LAB TOF at "cold" and "hot" rotational temperatures renders an excellent agreement with the experiment. Therefore, the increase of the backward scattering with T_{rot} seems to occur also experimentally, especially for v_f = 3 and v_f = 4.

4. Conclusions

Quasi-classical trajectory (QCT) calculations have been carried out for the reaction F+D_2 on an ab initio potential energy surface (PES) at the collision energies and initial rotational quantum numbers of the D_2 molecule necessary to simulate the experiments of Faubel et al. [43]. The high resolution of these experiments allows the determination of differential cross sections (DCS) with the highest precision ever achieved in the study of this reaction, and, therefore, constituting a very stringent test for dynamical calculations on ab initio potential energy surfaces.

It has been found as very important to compare not only with the experimental center-of-mass (CM) DCS, but also with the laboratory (LAB) angular distributions (AD) and time-of-flight (TOF) spectra, performing the necessary simulations and using the data obtained in the present QCT calculations.

In general, there is a good overall agreement between the experimental and the QCT theoretical results. Nevertheless, there are noticeable differences between the experimentally deduced and QCT DCS; the QCT calculations underestimate the backward scattering and the magnitude of the forward peak. The present calculations also fail in some instances, to accurately reproduce the observables in the LAB frame, yielding significant differences in the shape of the LAB AD.

The QCT calculations on the ab initio SW PES predict a very strong effect of the rotational temperature on the v_f resolved DCS, with a quite important increase of the backward and forward scattering. The experi-

mental TOF measurements at low and higher T_{rot}, at LAB angles corresponding to CM backward scattering, seem to corroborate, at least in part, this prediction. The simulation of the TOF spectra with the QCT v_f, j_f DCS gives a very good agreement with the experimental results.

It seems that some of the discrepancies between the present calculations and the measurements might be due to an insufficiency of classical mechanics. However, there are also indications that some disagreements might have their origin in inaccuracies of the PES. Accurate quantum mechanical (QM) calculations, at the collision energies and initial quantum states of the D_2 of the experimental measurements, need to be performed in the future in order to discriminate between these possibilities.

Acknowledgement

Special thanks should be paid to Klaus Stark and Joachim-H. Werner (University of Stuttgart) for letting us have their PES prior to publication. FJA is specially indebted to David Manolopoulos (Oxford University) not only for sharing with us all his QM results prior to publication, but also for many fruitful comments. The Spanish part of this project has been financed by the DGICYT of Spain (PB92-0219-C03). FJA and LB acknowledge the German-Spanish Scientific Exchange Program "Acciones Integradas" HA-074, HA-113 and HA-135. B. Martínez-Haya acknowledges support from the Human Capital and Mobility Programme. The work of Lev Y. Rusin in Göttingen was financed by a grant of the Deutsche Forschungsgemeinschaft.

References

[1] D.M. Neumark, A.M. Wodtke, G.N. Robinson, C.C. Hayden and Y.T. Lee, J. Chem. Phys. 82 (1985) 3045.
[2] D.M. Neumark, A.M. Wodtke, G.N. Robinson, C.C. Hayden, R. Shobatake, R.K. Sparks, T.P. Schafer and Y.T. Lee, J. Chem. Phys. 82 (1985) 3067.
[3] N.C. Blais and D.G. Truhlar, J. Chem. Phys. 76 (1982) 4490.
[4] S. Ron, M. Baer and E. Pollak, J. Chem. Phys. 78 (1983) 4414.
[5] M. Baer, J. Jellinek and D.J. Kouri, J. Chem. Phys. 78 (1983) 2962.
[6] J. Jellinek, M. Baer and D.J. Kouri, Phys. Rev. Letters 47 (1981) 1588.
[7] K.T. Lee and J.M. Bowman, J. Phys. Chem. 86 (1982) 2289.
[8] N. Abusalbi, C.L. Shoemaker and D.J. Kouri, J. Chem. Phys. 80 (1984) 3210.
[9] E.F. Hayes and R.B. Walker, J. Phys. Chem. 88 (1984) 3318.
[10] H.F. Schaefer III, J. Phys. Chem. 89 (1985) 5336.
[11] J.T. Muckerman, in: Theoretical chemistry. Advances and perspectives, Vol 6A, eds. H. Eyring and D. Henderson (Academic Press, New York, 1981) p. 1.
[12] T. Takayanagi and S. Sato, Chem. Phys. Letters 144 (1988) 191.
[13] R. Steckler, D.W. Schwenke, F.B. Brown and D.G. Truhlar, Chem. Phys. Letters 121 (1985) 475.
[14] D.W. Schwenke, R. Steckler, F.B. Brown and D.G. Truhlar, J. Chem. Phys. 84 (1986) 5706.
[15] G.C. Lynch, R. Steckler, D.W. Schwenke, A.J.C. Varandas and D.G. Truhlar, J. Chem. Phys. 94 (1991) 7136.
[16] S.L. Mielke, G.C. Lynch, D.G. Truhlar and D.W. Schwenke, Chem. Phys. Letters 213 (1993) 11; 217 (1994) 173 (E).
[17] J.M. Launay and M. Le Dourneuf, ICPEAC XVII Brisbane, July 1991, p. 549.
[18] J.M. Launay, Theoret. Chim. Acta 79 (1991) 183.
[19] F.J. Aoiz, V.J. Herrero, M.M. Nogueira and V. Sáez Rábanos, Chem. Phys. Letters 204 (1993) 359.
[20] F.J. Aoiz, V.J. Herrero, M.M. Nogueira and V. Sáez Rábanos, Chem. Phys. Letters 211 (1993) 72.
[21] F.J. Aoiz, L. Bañares, V.J. Herrero and V. Sáez Rábanos, Chem. Phys. Letters 218 (1994) 422.
[22] F.J. Aoiz, L. Bañares, V.J. Herrero and V. Sáez Rábanos, Chem. Phys. 187 (1994) 227.
[23] M.J. Berry, J. Chem. Phys. 59 (1973) 6229, and references therein.
[24] D.S. Perry and J.C. Polanyi, Chem. Phys. 12 (1976) 419, and references therein.
[25] E. Wurzberg and P.L. Houston, J. Chem. Phys. 72 (1980) 4811.
[26] R.F. Heidner III, J.F. Bott, C.E. Gardner and J.E. Melzer, J. Chem. Phys. 72 (1980) 4815.
[27] R. Atkinson, D.L. Baulch, R.A. Cox, R.F. Hampson Jr., S.A. Kerr and J. Troe, J. Phys. Chem. Ref. Data 18 (1989) 88.
[28] A. Weaver, R.B. Metz, S.E. Bradforth and D.M Neumark, J. Chem. Phys. 83 (1990) 5352.
[29] A. Weaver and D.M. Neumark, Faraday Discussions Chem. Soc. 91 (1991) 5.
[30] J.Z.H. Zhang, W.H. Miller, A. Weaver and D. Neumark, Chem. Phys. Letters 182 (1991) 283.
[31] S.E. Bradforth, D.W. Arnold, D.M. Neumark and D.E. Manolopoulos, J. Chem. Phys. 99 (1993) 6345.
[32] P.J. Knowles, K. Stark and H.-J. Werner, Chem. Phys. Letters 185 (1991) 555.
[33] F.J. Aoiz, L. Bañares, V.J. Herrero, V. Sáez Rábanos, K. Stark and H.-J. Werner, Chem. Phys. Letters 223 (1994) 215.
[34] K. Stark and H.-J. Werner, J. Chem. Phys., to be published.
[35] D.E. Manolopoulos, K. Stark, H.-J. Werner, D.W. Arnold, S.E. Bradforth and D.M. Neumark, Science 262 (1993) 1852.

[36] F.J. Aoiz, L. Bañares, V.J. Herrero, V. Sáez Rábanos, K. Stark and H.-J. Werner, J. Phys. Chem. 98 (1994) 10665.
[37] M. Faubel, S. Schlemmer, F. Sondermann and J.P. Toennies, J. Chem. Phys. 94 (1991) 4676.
[38] M. Faubel, L. Rusin, S. Schlemmer, F. Sondermann, U. Tappe and J.P. Toennies, J. Chem. Phys. 101 (1994) 2106.
[39] M. Faubel, B. Martínez-Haya, L.Y. Rusin, U. Tappe and J.P. Toennies, Chem. Phys. Letters 232 (1995) 197.
[40] J.F. Castillo, D.E. Manolopoulos, K. Stark and H.J. Werner, J. Chem. Phys., to be published.
[41] F.J. Aoiz, L. Bañares, V.J. Herrero, V. Sáez Rábanos, K. Stark and H.-J. Werner, J. Chem. Phys. 102 (1995) 9248.
[42] M. Faubel, B. Martínez-Haya, L.Y. Rusin, U. Tappe and J.P. Toennies, Z. Physik. Chem. 188 (1995) 197.
[43] M. Faubel, B. Martínez-Haya, L.Y. Rusin, U. Tappe, J.P. Toennies, F.J. Aoiz and L. Bañares, Chem. Phys. 207 (1996)227. preceding
[44] F.J. Aoiz, V.J. Herrero and V. Sáez Rábanos, J. Chem. Phys. 94 (1991) 7991.
[45] F.J. Aoiz, V.J. Herrero and V. Sáez Rábanos, J. Chem. Phys. 97 (1992) 7423.
[46] D.G. Truhlar and J.T. Muckerman, in: Atom–molecule collision theory, ed. R.B. Bernstein (Plenum Press, New York, 1979).
[47] V.M. Azriel, G.D. Billing, L.Yu. Rusin and M.B. Sevryuk, Chem. Phys. 195 (1995) 243.
[48] M.S. Child, Semiclassical mechanics with molecular applications (Clarendon Press, Oxford 1991).
[49] E. Rosenman and A. Persky, Chem. Phys. 195 (1995) 291.